Locomotion of a flapping flexible plate

Ru-Nan Hua, Luoding Zhu, and Xi-Yun Lu

Locomotion of a flapping flexible plate

Ru-Nan Hua,[1] Luoding Zhu,[2] and Xi-Yun Lu[1,a)]

[1]*Department of Modern Mechanics, University of Science and Technology of China, Hefei, Anhui 230026, China*
[2]*Department of Mathematical Sciences, Indiana University-Purdue University Indianapolis, 402 North Blackford Street, Indianapolis, Indiana 46202, USA*

The locomotion of a flapping flexible plate in a viscous incompressible stationary fluid is numerically studied by an immersed boundary-lattice Boltzmann method for the fluid and a finite element method for the plate. When the leading-edge of the flexible plate is forced to heave sinusoidally, the entire plate starts to move freely as a result of the fluid-structure interaction. Mechanisms underlying the dynamics of the plate are elucidated. Three distinct states of the plate motion are identified and can be described as forward, backward, and irregular. Which state to occur depends mainly on the heaving amplitude and the bending rigidity of the plate. In the forward motion regime, analysis of the dynamic behaviors of the flapping flexible plate indicates that a suitable degree of flexibility can improve the propulsive performance. Moreover, there exist two kinds of vortex streets in the downstream of the plate which are normal and deflected wake. Further the forward motion is compared with the flapping-based locomotion of swimming and flying animals. The results obtained in the present study are found to be consistent with the relevant observations and measurements and can provide some physical insights into the understanding of the propulsive mechanisms of swimming and flying animals. © *2013 AIP Publishing LLC*. [http://dx.doi.org/10.1063/1.4832857]

I. INTRODUCTION

Flapping plates are often used to mimic the motions of insect wings and fish fins for locomotion through fluids. Real wings and fins of animals are flexible[1–7] and can get deformed during flapping motion.[6–9] In general, the deformations of the wings or fins are generated by dynamic forces, elastic forces, and inertial forces due to accelerations. Meanwhile, the deformations also affect many aspects of the locomotion. To understand the role of flexibility in the flapping-based locomotion adopted by the swimming and flying animals, it is necessary to carry out relevant studies in detail.

The wings and fins in motion have complex behaviors which mainly depend on the internal distribution of the compliant components.[2,6] Because the wings lack internal muscles, there exist no actuators to realize internal control forces.[10] Consequently, the wings can deform passively in response to fluid forces while moving on its own. Similarly, the fins also experience the passive deformations against external hydrodynamic loads.[7] Meanwhile, the mechanical properties relevant to wings and fins have been studied. For example, Combes and Daniel[4,5] have addressed the relationship between venation pattern and wing flexibility through measuring the flexural stiffness of wing and quantifying the wing venation. Alben *et al.*[11] have experimentally examined the mechanical properties of fin rays that allow the control of fin shape and stiffness in response to external forces. Such properties of wings and fins have provided a physical basis for establishing a reliable model for experimental and numerical investigations.

To understand the fundamental principles and potential applications of the flapping-based locomotion of swimming and flying animals, a variety of experimental,[12–17] theoretical,[18–20] and

---

a)Electronic mail: xlu@ustc.edu.cn

computational[21–30] studies have been conducted. In these works, the foil-like structures for modeling wings or fins are essentially rigid and thus the flapping motions of the entire solid structure are prescribed. Some studies on flapping flexible foils or plates have also been carried out experimentally[31,32] and numerically[33–36] to investigate the effects of flexibility on the dynamic behaviors of the fluid-solid system.

For animals in a steady state of free flight or swimming, the mean thrust generated balances the resistance experienced by the surrounding fluid. Thus, it is necessary to study the dynamical behaviors relevant to the free motion. We should mention that the physical models considered in the works cited above are an object immersed in a *given* uniform incoming flow. Wu[37] has indicated that the fluid dynamics of a flow past a stationary object is different from a free moving object in a stationary fluid. Recently, some efforts have been made to investigate the locomotion of flapping flexible foils or plates in a stationary fluid. Tytell *et al.*[38] has performed modeling and simulation of the lamprey swimming in two dimensions. Spagnolie *et al.*[39] and Zhang *et al.*[40] have studied the dynamics of a heaving plate with passive pitching to understand the role of flexibility in flapping locomotion. However, since the instantaneous shape of an elastic structure in free motion depends on the local passive deformation due to the fluid-structure interaction, a model of a flexible wing moving passively in a stationary viscous fluid is needed for the understanding of the locomotion behaviors of the flexible wings or fins.

In the present study, we consider a flexible plate with its leading-edge being forced to heave sinusoidally in a stationary fluid. As a result of fluid-structure interaction, the plate begins to move freely in the fluid. The coupled motions of the fluid and plate are numerically solved by an immersed boundary-lattice Boltzmann method for the fluid and by a finite element method for the plate. The purpose of this study is to achieve an improved understanding of the fundamental mechanisms relevant to the locomotion of a flapping flexible plate with applications to animal swimming and flying.

This paper is organized as follows. The physical problem and mathematical formulation are presented in Sec. II. The numerical method and validation are described in Sec. III. Detailed results are discussed in Sec. IV and concluding remarks are addressed in Sec. V.

II. PHYSICAL PROBLEM AND MATHEMATICAL FORMULATION

A two-dimensional model of the flapping plate is considered. As shown in Fig. 1, a flexible plate with length c is immersed in a stationary viscous incompressible fluid. The leading-edge is forced to heave sinusoidally with amplitude A_0 and frequency f in the vertical direction. Similar to the treatment of the previous studies,[33,35] the forced motion of the leading-edge is described by

$$h(t) = A_0 \cos(2\pi f t). \tag{1}$$

As a result of the interplay of the internal elasticity, the leading-edge forcing, and the forces exerted by the surrounding fluid, the plate starts to move freely and passively in the stationary fluid. The passive pitching angle α can be defined as the angle between the x-axis and the secant connecting the leading-edge to the trailing-edge. Note that the active pitching angle is zero in our model; it means that only the leading-edge of the plate is restricted with its vertical motion being prescribed, the remainder of the plate can move freely in the entire fluid domain.
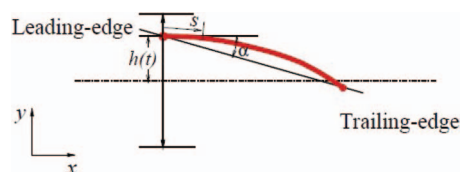
FIG. 1. Sketch of a model for the locomotion of a flapping flexible plate. When the leading-edge is forced to heave vertically and sinusoidally, the plate deforms passively and moves freely.

The plate is assumed to be a two-dimensional thin elastic beam and its dynamics is governed by the nonlinear partial differential equation[41,42]

$$\rho_l \frac{\partial^2 X}{\partial t^2} - \frac{\partial}{\partial s}\left[T(s)\frac{\partial X}{\partial s}\right] + EI\frac{\partial^4 X}{\partial s^4} = F_s, \tag{2}$$

where s is the Lagrangian coordinate along the plate, X is the position vector of the plate, ρ_l is the structural linear mass density, $T(s) = Eh(|\frac{\partial X}{\partial s}| - 1)$ is the tension with Eh being the structural stretching rigidity, and EI is the structural bending rigidity. The plate is subject to the hydrodynamic load

$$F_s = [\sigma] \cdot n, \tag{3}$$

where n is the upward norm and $[\sigma]$ is the difference in the fluid stress tensor across the plate. The boundary conditions for the plate are

$$y_L = h(t), \frac{\partial X}{\partial s} = (1, 0) \tag{4}$$

at the leading-edge, and

$$T = 0, \frac{\partial^2 X}{\partial s^2} = (0, 0), \frac{\partial^3 X}{\partial s^3} = (0, 0) \tag{5}$$

at the trailing-edge.

The incompressible Navier-Stokes equations are used to describe the flow dynamics

$$\frac{\partial v}{\partial t} + v \cdot \nabla v = -\frac{1}{\rho}\nabla p + \frac{\mu}{\rho}\nabla^2 v, \tag{6}$$

$$\nabla \cdot v = 0, \tag{7}$$

where v is the velocity, p the pressure, ρ the density of the fluid, and μ the dynamic viscosity. The flow is initially quiescent. The velocity boundary condition for the fluid is imposed on the plate,

$$v = \frac{\partial X}{\partial t}. \tag{8}$$

The reference quantities c, f, and ρ are chosen to non-dimensionalize the above mathematical formulation. The dimensionless parameters are defined as follows: the heaving amplitude $A = A_0/c$, the frequency Reynolds number $Re_f = \rho f c^2/\mu$, the linear mass density ratio of the plate and the fluid $M = \rho_l/\rho c$, the bending stiffness $K = EI/\rho f^2 c^5$, and the stretching stiffness $S = Eh/\rho f^2 c^3$.

III. NUMERICAL METHOD AND VALIDATION

A. Numerical method

The governing equations of the fluid-plate problem are solved numerically by an immersed boundary-lattice Boltzmann method for the fluid flow and a finite element method for the motion of the flexible plate. The immersed boundary (IB) method has been extensively applied to problems involving moving boundaries immersed in a viscous fluid flow.[43,44] When the IB method is used to treat flow-structure interaction, a body force f is added into the right hand of Eq. (6). The Lagrangian interaction force between the fluid and the immersed boundary can be calculated by the feedback law[45–47]

$$F_s(s, t) = \alpha \int_0^t [V_f(s, t') - V_s(s, t')]dt' + \beta[V_f(s, t) - V_s(s, t)], \tag{9}$$

where α and β are free parameters and are selected based on the previous studies[48,49] and V_f is the fluid velocity at the position of the body obtained by interpolation

$$V_f(s, t) = \int_\Gamma v(x, t)\delta(x - X(s, t))dx. \tag{10}$$

Then, the Eulerian body force can be calculated as

$$f(\boldsymbol{x}, t) = -\int_{\Gamma} \boldsymbol{F}_s(s, t)\delta(\boldsymbol{x} - \boldsymbol{X}(s, t))\mathrm{d}s. \tag{11}$$

The interaction forces $\boldsymbol{F}_s(s, t)$ and $f(\boldsymbol{x}, t)$ obtained by Eqs. (9) and (11) are used in Eqs. (2) and (6), respectively.

Due to its relative simplicity and efficiency, the lattice Boltzmann equation (LBE) has been widely used to simulate complex flows as an alternative to conventional numerical methods for the Navier-Stokes equations.[48,50–52] The LBE with the BGK model is

$$f_i(\boldsymbol{x} + \boldsymbol{e}_i\Delta t, t + \Delta t) - f_i(\boldsymbol{x}, t) = -\frac{1}{\tau}[f_i(\boldsymbol{x}, t) - f_i^{eq}(\boldsymbol{x}, t)] + \Delta t F_i, \tag{12}$$

where τ is the non-dimensional relaxation time associated with fluid viscosity, Δt is the time increment, and $f_i(\boldsymbol{x}, t)$ is the distribution function for particles with velocity $\boldsymbol{e}_i$ at position $\boldsymbol{x}$ and time t. The equilibrium distribution function f_i^{eq} and the forcing term F_i[53,54] are defined as

$$f_i^{eq} = \omega_i \rho \left[1 + \frac{\boldsymbol{e}_i \cdot \boldsymbol{v}}{c_s^2} + \frac{\boldsymbol{v}\boldsymbol{v} : (\boldsymbol{e}_i\boldsymbol{e}_i - c_s^2\boldsymbol{I})}{2c_s^4} \right], \tag{13}$$

$$F_i = \left(1 - \frac{1}{2\tau} \right) \omega_i \left[\frac{\boldsymbol{e}_i - \boldsymbol{v}}{c_s^2} + \frac{\boldsymbol{e}_i \cdot \boldsymbol{v}}{c_s^4}\boldsymbol{e}_i \right] \cdot \boldsymbol{f}, \tag{14}$$

where ω_i is the weighting factor and c_s is the speed of sound. The variables velocity $\boldsymbol{v}$ and mass density ρ can be obtained by the distribution functions

$$\rho = \sum_i f_i, \tag{15}$$

$$\rho\boldsymbol{v} = \sum_i \boldsymbol{e}_i f_i + \frac{1}{2}\boldsymbol{f}\Delta t. \tag{16}$$

A multi-scale analysis performed on the LBE recovers the Navier-Stokes equations. A multi-block lattice Boltzmann technique[55,56] is employed to solve our problem for improving computational efficiency.

Equation (2) for the deformable plate is discretized by a finite element method and the motion of the plate is handled by the corotational scheme.[57,58] In this scheme, a local coordinate system is envisioned to move with each discrete element, and the element behaves linearly relative to the moving coordinate system. Consequently, the nonlinearity of the problem goes to the coordinate transformation.

Based on our careful examinations and validations shown below, the computational domain for fluid flow is chosen as $-64 \leq x \leq 64$ and $-32 \leq y \leq 32$. The finest lattice spacing is $c/128$ in the region close to the plate and the coarsest spacing is $c/32$ elsewhere. The time step is $T/12800$ with $T = 1/f$ being the flapping period. Dirichlet boundary condition $\boldsymbol{v} = 0$ is used at the top and bottom boundaries, and Neumann boundary condition $\partial\boldsymbol{v}/\partial x = 0$ is used at the inlet and the outlet. For the present problem, a finite moving computational domain[40,51,52] is employed in the x-direction to allow the plate to move horizontally for a sufficiently long time. Every time the plate travels one lattice unit on the coarse grid in the horizontal direction, the computational domain is shifted, i.e., one layer being added at the inlet and another layer being removed at the outlet.[40]

B. Validation

To validate the numerical method used in the present study, three typical test cases are considered here. The first two tests are hovering-wing problems, with one wing being rigid and the other being flexible. Besides the heaving motion Eq. (1), a pithing motion is also given as $\alpha(t) = \beta\sin(2\pi ft)$ with β the angle amplitude. These problems were already studied numerically by Yin and Luo.[59] The dimensionless parameters are as follows: $\beta = \pi/4$, $A = 1.4$, and $Re_f = 8.53$ for the rigid case; $\beta = 0$, $A = 1.25$, $Re_f = 19.1$, $K = 12.77$, and $M = 1.0$ for the flexible case. The lift and drag
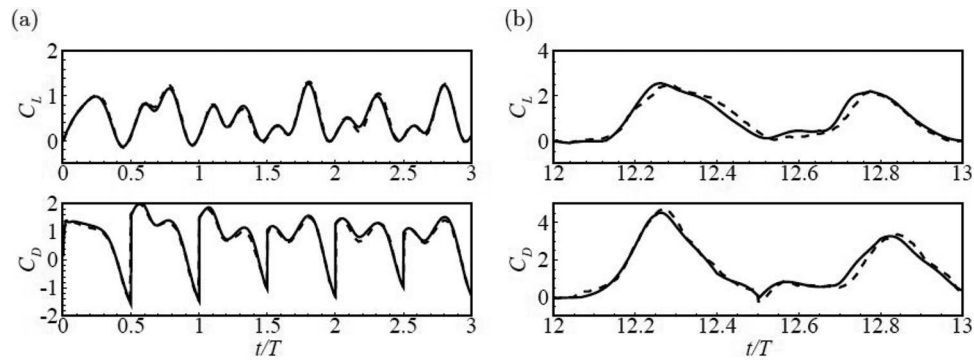
FIG. 2. Lift and drag coefficients from the our simulation (solid line) and from the previous work[59] (dashed line) for hovering of (a) a rigid wing and (b) a flexible wing.

coefficients obtained in our simulation are shown in Fig. 2. It is seen that our calculated results are in good agreement with the previous study.[59]

The third test is a problem of free flapping body which has been studied experimentally[14] and numerically.[27,40] The physical model is an elliptic foil being flapped vertically within a viscous incompressible fluid. Similarly to our case, the foil begins to move freely in the fluid along the horizontal direction. Here a typical set of parameters is used: the thickness ratio is 0.1, the flapping amplitude is 0.5, and the mass density ratio is 32. Figure 3 shows the mean horizontal speed during the steady locomotion on the plot of the movement Reynolds number Re_U versus the flapping Reynolds number Re_A. The flapping Reynolds number is defined as $Re_A = \rho f A_0 c/\mu$, which is related to the frequency Reynolds number Re_f by $Re_A = Re_f A$. The movement Reynolds number is defined as $Re_U = \rho U c/\mu$, where the propulsive speed U is the horizontal velocity of the foil after it begins the steady motion. It is identified that our computational results agree well with the previous data.[40]

In addition, the relevant codes used for the present study have been also validated in our previous works.[48,49,56,60] The numerical method has been applied with success to a wide range of flows such as the insect normal hovering flight with ground effect,[48] hydrodynamic interaction of elastic filaments,[60] and viscous flow past three filaments in side-by-side arrangement.[49]

IV. RESULTS AND DISCUSSION

In this section, we present some typical results on the dynamics of the flapping flexible plate and discuss the intrinsic connections between our results and the flapping-based locomotion of swimming and flying animals. Motivated by the measurements of animal locomotion,[61–68] the governing parameters used in our study are as follows: $A = 0.125–1.0$, $K = 0.1–1000$, $M = 0.5–4.0$,
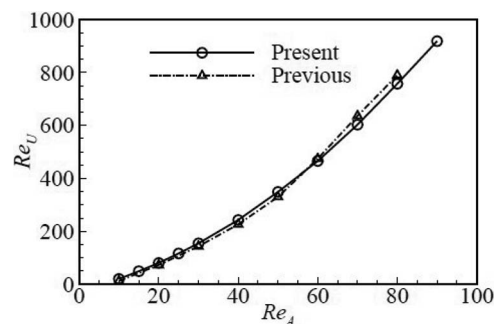
FIG. 3. Comparison of the present result and previous data[40] for the forward Reynolds number Re_U versus the flapping Reynolds number Re_A during the steady locomotion for flapping flight of an elliptic foil.

and $Re_f = 80–120$. Unless otherwise stated, the Reynolds number and the mass density ratio are $Re_f = 100$ and $M = 2.0$.

A. Three states of the plate movement

Based on a series of simulations using a wide range of parameters, we have identified three typical states of the plate motion due to the fluid-structure interaction: backward motion (BM) where the plate moves along the x-direction, forward motion (FM) where the plate moves along the negative x-direction, and irregular motion (IM) where the plate moves back and forth about its initial position.

The propulsive speed of the plate is addressed first. Figures 4(a)–4(c) show the time history of the instantaneous propulsive speed $u(t)$, i.e., the x-component of the velocity of the plate mass center,[24] for three typical cases corresponding to the three distinct states of the plate motion. Note that all of the parameters for the three cases are the same except for the plate rigidity. It is chosen as $K = 0.4$, 1.5, and 10 to illustrate the influence of flexibility on the plate movement. In the BM state, the plate moves towards the trailing-edge with speed $u(t) > 0$ after it reaches a steady state. In the FM state, the plate moves towards the leading-edge with speed $u(t) < 0$. In the IM state, the plate moves forward and backward randomly with its speed being switched between $u(t) > 0$ and $u(t) < 0$. Further, Figs. 4(d)–4(f) show the power spectrum density (PSD) of the propulsive speed for the three cases. The power spectra of $u(t)$ in Figs. 4(d) and 4(e) for the BM and FM states exhibit a single high peak. For the IM state, Fig. 4(f) shows a broadband spectrum, indicating a non-periodic
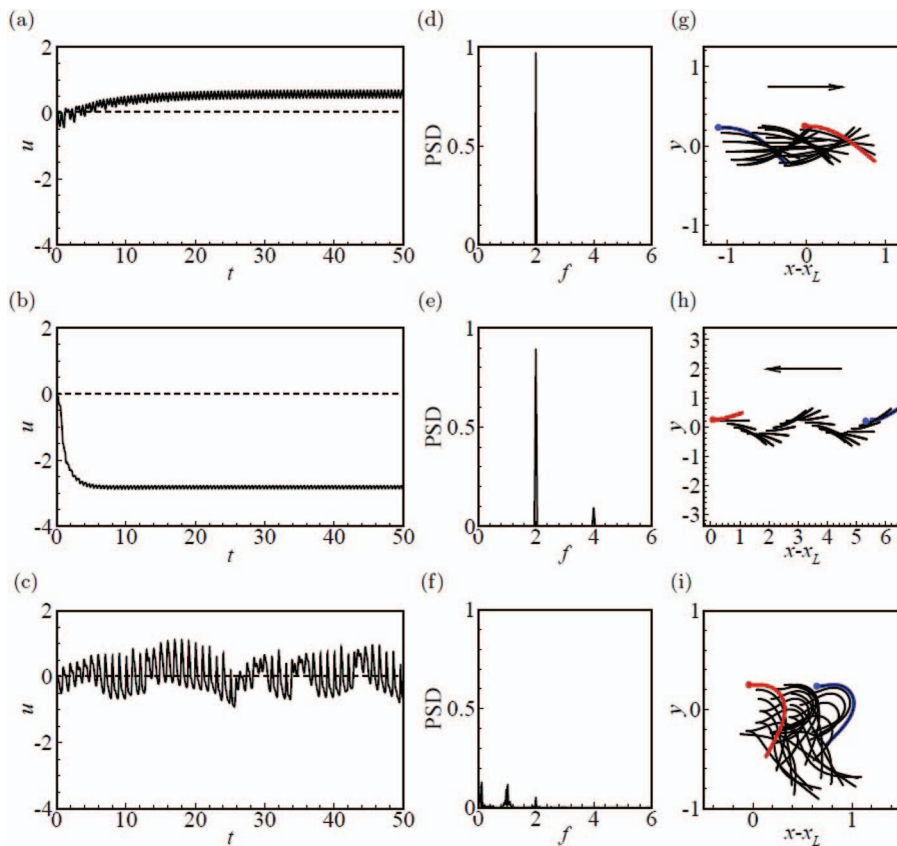
FIG. 4. Behaviors of the propulsion and deformation of the plate: (a)–(c) the instantaneous propulsive speed $u(t)$, (d)–(f) the corresponding power spectrum density, and (g)–(i) the envelops of the plate in two flapping cycles ($t = 40 − 42$) for the three distinct states with $A = 0.25$ and [(a), (d), (g)] $K = 1.5$, [(b), (e), (h)] $K = 10.0$, and [(c), (f), (i)] $K = 0.4$, corresponding to BM, FM, and IM, respectively.
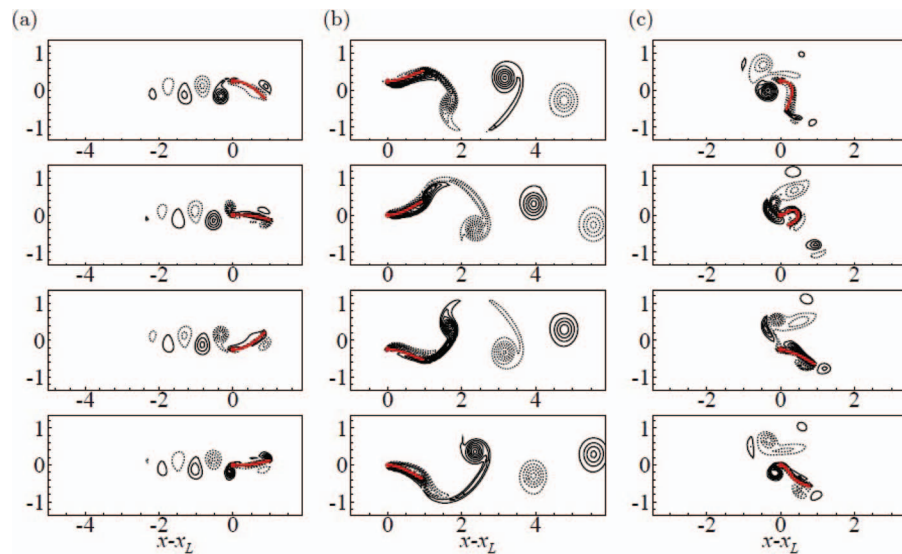
FIG. 5. The instantaneous vorticity contours for one flapping cycle at the phases 0/4T, 1/4T, 2/4T, and 3/4T from top row to bottom one for the three distinct states: (a) $K = 1.5$, (b) $K = 10.0$, and (c) $K = 0.4$. Solid lines denote positive values and dashed lines negative values for the vorticity contours.

behavior of the irregular motion state. Moreover, a similar IM state for the free motion of flapping *rigid* body has also been observed numerically[25] and experimentally.[39]

Illustrating the deformation of the plate due to the fluid-structure interaction, Figs. 4(g)–4(i) show the envelopes of the flexible plate during two flapping cycles. It is seen that the envelopes for the three motion states are obviously different and are associated with the propulsive performance of the plate. Another form of envelope will be analyzed in the following section, which is related to the formation of deflected wake for the FM state.

The corresponding instantaneous vorticity contours for one flapping cycle are shown in Figs. 5(a)–5(c) to exhibit the vortical structures induced by the plate motion. For the BM and FM states, the vortex wake occurs on the opposite direction of the plate mean velocity to form the reverse von Kármán vortex street behind the plate. Actually, the reverse von Kármán vortex street, which is responsible for thrust production of the flapping plate, has already been observed experimentally and numerically in flapping rigid foils and swimming fish.[16,25,38,69] As the plate moves at random in the IM state, a jumbled vortex structure is observed around the plate.

Further, an overview of the three distinct motion regions in the K–A plane is shown in Fig. 6. Note that the FM state covers a majority of the K–A plane while the BM state covers a minority of the plane. When the heaving amplitude is large enough (say $A > 0.80$), only the FM and IM states occur; when the heaving amplitude is small enough (say $A < 0.15$), only the FM state appears. We also notice that the critical value of K separating the regions increases as A increases.
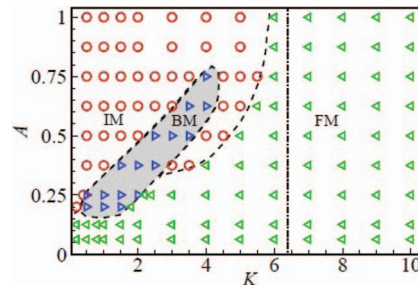
FIG. 6. Overview of the three typical motion regions in the K–A plane. Symbols $\triangleright$, $\triangleleft$, and $\circ$ represent the backward, forward, and irregular motions, respectively. The vertical dotted dashed line represents the frequency ratio $\bar{f} = 1$.
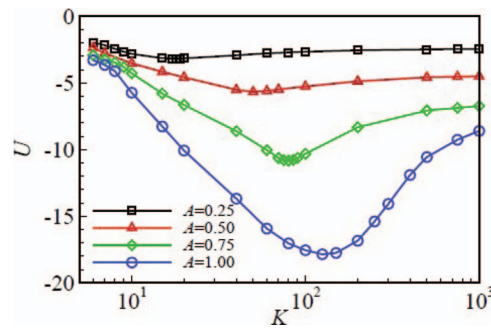
FIG. 7. The mean propulsive speed U versus the bending stiffness K for four typical values of heaving amplitude A.

To analyze the dynamical responses of the flapping flexible plate, another important parameter, i.e., the frequency ratio $\bar{f}$, is introduced.[40,59,70] The frequency ratio is defined as $\bar{f} = f_n/f$, where $f_n = k_n^2/(2\pi c^2)\sqrt{EI/\rho_l}$ is the frequency of the first natural mode of the flexible plate with $k_n = 1.8751$.[71] Here, the frequency ratio can be expressed as $\bar{f} = k_n^2/(2\pi)\sqrt{K/M}$. Zhang *et al.*[40] have used a torsion spring to model the flexibility effect of a flapping rigid plate (i.e., a lumped-torsional-flexibility model) and have found that the two distinct regions (BM and FM) were determined by this frequency ratio: the BM region corresponding to $\bar{f} < 1$ and the FM region corresponding to $\bar{f} > 1$. We plot the $\bar{f} = 1$ line in Fig. 6. It is seen that the line $\bar{f} = 1$ does not describe the border between the FM and BM regions in the A–K plane for the flexible plate. The border separating the FM and BM regions in the present study is far more complex than the line $\bar{f} = 1$. This indicates that the present problem is inherently more complicated. The model used by Zhang *et al.*[40] was rigid while the plate in this study is flexible and the fluid-structure interaction involving a deformable body is in general more complicated.

B. Dynamical behaviors and propulsive properties

The plate motion as a result of the fluid-structure interaction is closely related to the flapping-based locomotion of swimming and flying animals. The dynamical behaviors and propulsive properties in the FM region are further investigated in terms of the mean propulsive speed, the propulsive efficiency, the passive pitching angle, the elastic potential energy of the flexible plate, and the Strouhal number.

To understand the dynamical responses of the plate due to the fluid-plate interaction, Fig. 7 shows the mean propulsive speed U versus the bending rigidity K for several heaving amplitudes, where U is obtained by an average in time of $u(t)$ during steady locomotion. It is seen that the profiles of U are all concave up for different heaving amplitudes. For each amplitude A, the speed U decreases as K increases first, then reaches a minimum (corresponding to the maximum of the forward speed $|U|$), and finally approaches a constant as K increases further. Note that the motion of the flexible plate tends to the motion of the rigid one at large value of K, e.g., $K = 1000$. Besides, the speed U is an increasing function of the amplitude A. We speculate that the existence of the maximum of the forward speed (denoted by U_m) implies the existence of an optimal plate flexibility (denoted by K_U). For comparison, Table I lists K_U, U_m, and U_c for the four amplitudes, where U_c represents the forward speed in the rigid case. It is seen that the optimal forward speeds of the flexible plate are

TABLE I. The optimal K_U, the corresponding maximum forward speed U_m, and that of the approximate rigid case U_c for different A.

A	0.25	0.50	0.75	1.00
K_U	18.0	50.0	80.0	125.0
U_m	3.16	5.66	10.82	17.86
U_c	2.46	4.50	6.74	8.60
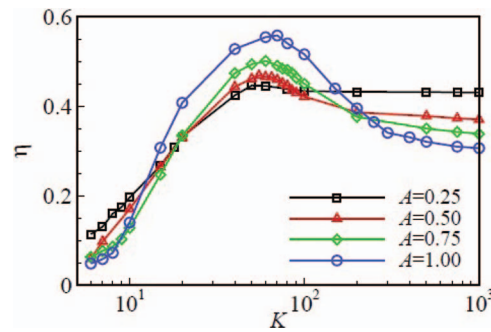
FIG. 8. The propulsive efficiency η versus the bending stiffness K.

substantially greater than those of the corresponding rigid plate for several amplitudes, indicating that the flexibility can remarkably improve the performance of forward propulsion.

As the plate spontaneously propels itself in the horizontal direction in the FM state, the mean thrust becomes zero.[40,72] Then the Froude propulsive efficiency[13,18] vanishes, which is no longer suitable for measuring the propulsive efficiency. To characterize the propulsive efficiency of a body in free motion, the ratio of the kinetic energy of the forward motion of the body and the work done by the deforming body over one flapping cycle has been employed by Zhang et al.[40] and Kern and Koumoutsakos.[26] The amount of the work is computed as a time integral of the power performed by the surface of the body on the surrounding fluid. Then, the propulsive efficiency for the locomotion of flexible plate is expressed as[26,40]

$$\eta = \frac{\frac{1}{2}MU^2}{\int_{t_0}^{t_0+T} \int_0^c \boldsymbol{F}_r(s,t) \cdot \frac{\partial X(s,t)}{\partial t} \mathrm{d}s \mathrm{d}t}, \qquad (17)$$

where $\boldsymbol{F}_r(s,t)$ represents the force on the surrounding fluid by the plate and can be expressed as $\boldsymbol{F}_r(s,t) = -\boldsymbol{F}_s(s,t)$.

Figure 8 shows the propulsive efficiency η versus the bending stiffness K for four typical heaving amplitudes. For a given heaving amplitude, the efficiency η first increases to a maximum and then decreases gradually as K increases. Similarly, there exists an optimal plate flexibility K_η corresponding to the maximal propulsive efficiency η_m. Table II lists K_η, η_m, and η_c for four typical values of amplitude A, where η_c represents the efficiency of the rigid case. It is seen that the optimal efficiency of the flexible plate is greater than that of the rigid plate. Thus, from Figs. 7 and 8 as well as Tables I and II, we can reasonably conclude that a suitable amount of structure flexibility can improve the propulsive speed and efficiency and hence is beneficial to animal locomotion in a viscous fluid.

All of the above results are obtained from simulations using different plate bending modulus and heaving amplitude but fixed frequency Reynolds number ($Re_f = 100$) and plate linear mass density ($M = 2$). To gauge the effects of the parameters Re_f and M on the propulsive speed and efficiency, we further perform some simulations using different values of Re_f and M. The typical results are shown in Fig. 9. It is identified from Figs. 9(a) and 9(b) that the forward speed $|U|$ decreases with the increases of the mass density M but the propulsive efficiency η increases with M. The propulsion of the flapping plate is closely related to the reverse von Kármán vortex street which

TABLE II. The optimal K_η, the corresponding maximal propulsive efficiency η_m, and that of the corresponding rigid case η_c for different values of A.

A	0.25	0.50	0.75	1.00
K_η	50.0	53.0	60.0	70.0
η_m	0.446	0.468	0.501	0.558
η_c	0.430	0.370	0.338	0.306
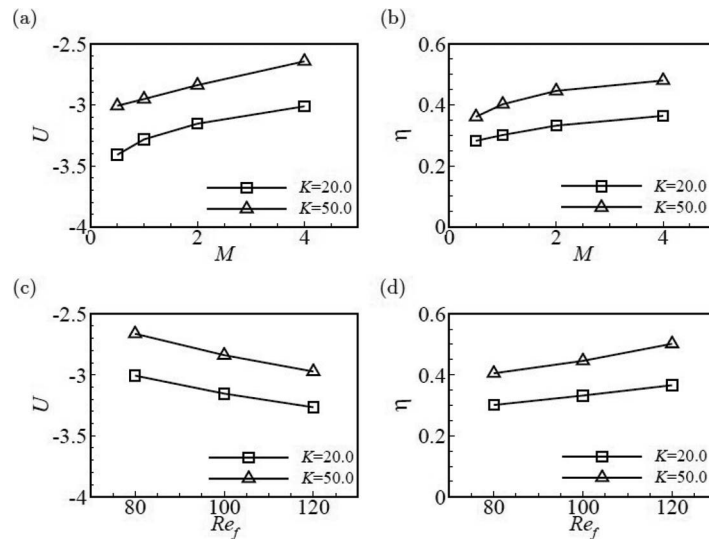
FIG. 9. Propulsive speed U [(a), (c)] and propulsive efficiency η [(b), (d)] versus the linear density ratio M for $A = 0.25$ and $Re_f = 100$ in [(a), (b)] and versus the Reynolds number for $A = 0.25$ and $M = 2.0$ in [(c), (d)].

is not sensitive to the plate mass density in a certain range. Given the amount of propulsion, the plate acceleration is inversely proportional to its mass. As a consequence, the terminal forward speed of the plate decreases as its mass density increases. Moreover, it has been indicated that the mass plays a stabilizing role in the fluid-flexible-structure system.[73] This may imply that a more massive flexible structure induces less local motion of the structure which causes energy dissipation. Thus, the decreased total energy consumption due to the reduced energy waste of the fluid-plate system is therefore beneficial to propulsive efficiency. From Figs. 9(c) and 9(d), it is seen that as Re_f increases the forward speed and efficiency increase, which is associated with the reduction of viscous drag of the plate for the parameters considered.

As the plate is flexible, it can store elastic potential energy because of the fluid-plate interaction. The elastic potential energy of the plate is expressed as $E_p(t) = 1/2K \int_0^c |\partial^2 X/\partial s^2|^2 ds$.[74] Note that the elastic potential due to stretching is neglected because it is at least one order of magnitude lower than the bending energy based on our test and previous study.[49] Here we use the elastic potential energy of a cantilever beam denoted by E_s[75] to normalize it. Then the normalized elastic potential energy is represented as $E_r = \bar{E}_p/E_s$ with $\bar{E}_p = 1/T \int_0^T E_p(t) dt$. Figure 10 shows the elastic potential energy versus the bending stiffness for several flapping amplitudes. It is identified that the large value of E_r for each amplitude corresponds to the high propulsive efficiency in Fig. 8.

Further, we analyze the passive pitching angle which is related to the deformation of the flexible plate subject to the fluid-structure interaction. Moreover, the pitching angle is closely associated
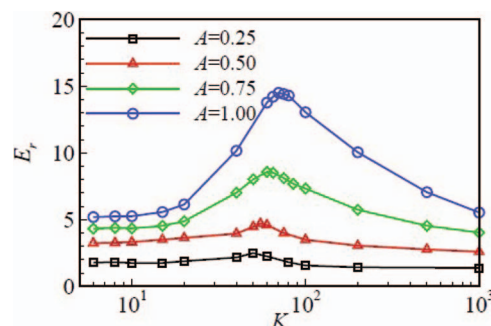
FIG. 10. The normalized elastic potential energy E_r versus the bending stiffness K.
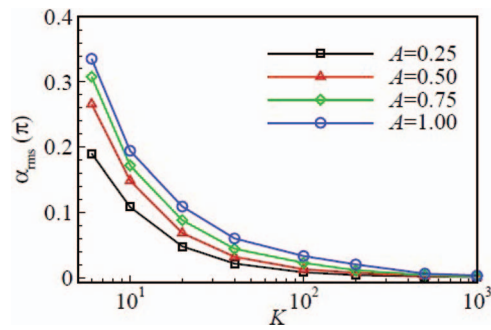
FIG. 11. The rms value of passive pitching angle α_{rms} versus the bending stiffness K.

with hydrodynamic performance for an actively forced flapping rigid foil or plate.[12,13,69] Figure 11 shows the root-mean-square (rms) value of the passive pitching angle α versus the bending rigidity K for several values of amplitude A. The passive pitching angle is caused by the delayed motion of the free end of the plate relative to the constrained end, which can be presented by the displacement in the y-direction. It is seen from Fig. 11 that larger heaving amplitude or smaller bending modulus (i.e., more flexible) causes more delay at the free end, and therefore results in larger pitching angle.

The kinematics of flapping-based locomotion is usually well described by the Strouhal number which is defined as $St = A_w f/U$. Here A_w is the width of the wake which may be taken as the maximum excursion of the plate trailing-edge or twice of the amplitude, i.e., $A_w = 2A$.[12,27] As shown in Fig. 12, the Strouhal numbers of the majority of our simulations fall into the range of $0.2 < St < 0.4$, which is consistent with the region of high propulsive efficiency of the flapping-based locomotion.[65,69] Moreover, the Strouhal number is known to describe a well-defined series of regimes for vortex growth and shedding of a flapping body, which will be discussed in the following subsection.

C. Vortical structures of normal and deflected wake

The vortical structure in the wake is related to the propulsive properties of a flapping wing.[17,23] Based on the analysis of vorticity dynamics,[76,77] we have found that the force and power of the flapping plate are dominated by the attached vorticity and the local vortical structure close to the plate. Therefore, the vortical structure is further discussed here. As shown in Fig. 5, a reverse von Kármán vortex street is formed behind the flapping plate in the FM and BM states, and a jumbled vortical structure is observed around the plate in the IM state.

For the FM region, our simulations reveal two kinds of wakes behind the plate. One is the normal wake and the other is the deflected wake in which the wake behind the plate is biased with respect to the symmetric axis of the forced motion of the plate, rather than a normal wake such as the von Kármán street behind a body.
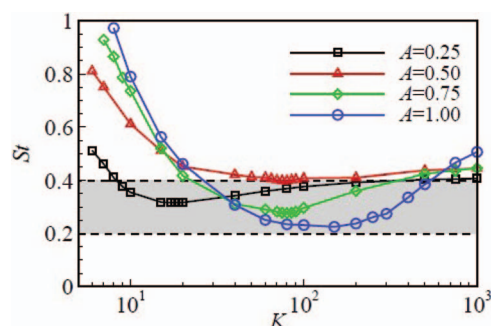
FIG. 12. The Strouhal number St versus the bending stiffness K.
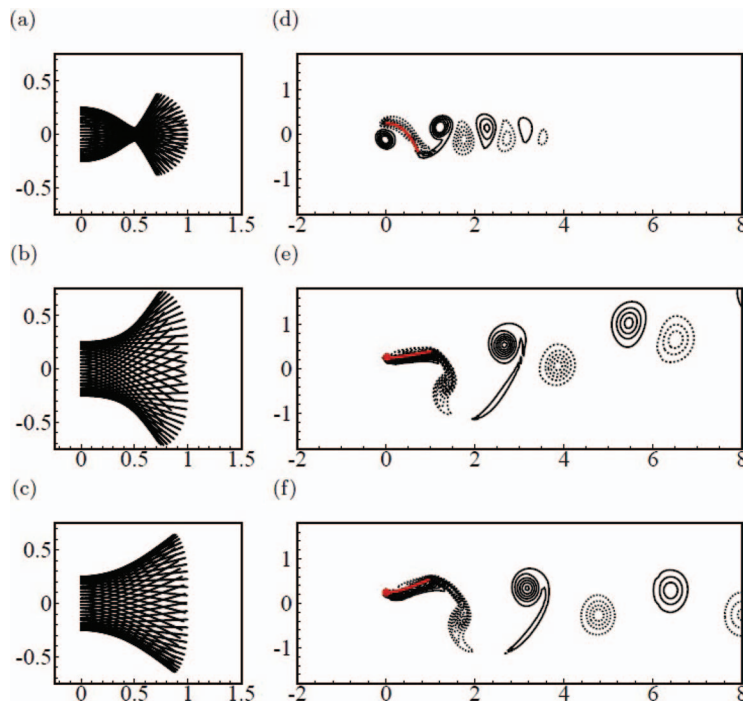
FIG. 13. (a)–(c) Envelopes of the flexible plate in one flapping cycle ($t/T = 40 - 41$) and (d)–(f) the corresponding instantaneous vorticity contours at $t/T = 40$ for $A = 0.25$ and $K = $ [(a), (d)] 2.8, [(b), (e)] 7, and [(c), (f)] 10. Solid lines denote positive values and dashed lines denote negative values. The envelopes of the plate are plotted in the frame moving with the leading-edge in the horizontal direction.

To demonstrate the wake structure and the plate deformation, Fig. 13 shows the envelopes of the flexible plate in one flapping cycle and the instantaneous vorticity contours for three typical cases with $A = 0.25$ and $K = 2.8$, 7, and 10. As the mean forward speed given in Fig. 7 increases with the K from 2.8 to 10 at $A = 0.25$, the longitudinal distance between two neighboring vortical structures increases as shown in Fig. 13. For $K = 7$ which lies in the deflected wake region, it is seen from Fig. 13(b) that the wake is upwardly deflected in the downstream. Further, our simulations reveal that the initial heaving direction of the plate leading-edge decides the deflected direction, i.e., upward or downward in the downstream. A non-zero mean lift is generated because of the deflection of the reverse von Kármán vortex street. For comparison, the mean lift coefficient is calculated as follows: $\bar{C}_L = 1.456$ for $K = 7$ for the deflected wake and $\bar{C}_L = 0.012$ for $K = 10$ for the normal wake.

It is natural to inquire whether the wake deflection is caused by the deflection in the motion of the flapping plate. To address this issue, the envelopes of the flapping flexible plate for one flapping cycle are shown in Fig. 13, where the x-position of the leading-edge is shifted to the same position. It is interesting to notice that the envelope for the deflected wake case is still nearly symmetric with respect to the axis of plate motion, just looking like the case of the normal wake. Actually, deflected vortex streets behind a flapping rigid foil with symmetric motion in a uniform flow have been observed experimentally[16,17,78] and numerically.[78,79] Therefore, it is reasonable to expect that the wake deflection of symmetric plate flapping motion may account for the generation of the mean lift and thrust in the flapping-based locomotion of animals.

To have a better understanding of the deflected vortex street, Fig. 14 shows the time history of the propulsive speed in one flapping cycle and the corresponding PSD for the three typical cases shown in Fig. 13. As expected, the non-dimensional frequency corresponding to the peak in the PSD is $f = 2$ for $K = 2.8$ and 10, while a subharmonic frequency $f = 1$ occurs for $K = 7$. It means that the plate travels a different distance in the two half-cycles of a whole cycle in the case of $K = 7$. This further results in the inequality in the longitudinal distance between the two neighboring vortical structures. Note that such a longitudinal distance disparity is absent in the case of normal wake.
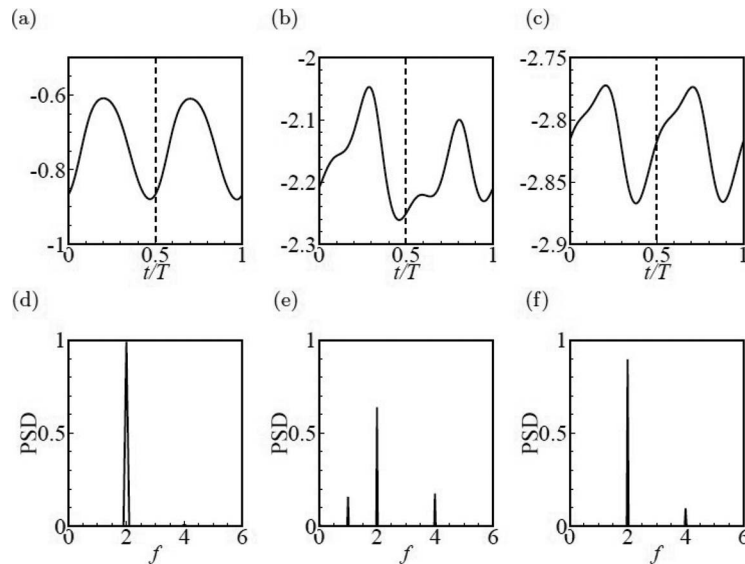
FIG. 14. Time history of propulsive speed $u(t)$ in one flapping cycle and the corresponding PSD for $A = 0.25$ and $K = [$(a), (d)$]$ 2.8, $[$(b), (e)$]$ 7, and $[$(c), (f)$]$ 10.

Here we can calculate the distance difference by $L_d = |(\int_0^{T/2} u\mathrm{d}t - \int_{T/2}^{T} u\mathrm{d}t)/(\int_0^T u\mathrm{d}t)| \times 100\%$. The results are $L_d = 0.88\%$ for $K = 7$ and $L_d = 0.0037\%$ for $K = 10$. Although the disparity is small, the distance difference of the deflected wake is significantly greater than that of the normal wake, resulting in the deflected evolution of the vortices in the downstream of the flapping plate.

To summarize our findings on the two kinds of wakes, Fig. 15 shows an overview of the normal and deflected wake regions in the A–K plane. Note that the range of the bending rigidity K for the deflected wake is around 7 (the frequency ratio $\bar{f}$ is around 1) which is much lower than the range of $K \sim O(10^2)$ for the optimal propulsive speed and efficiency.

D. Comparison with the flapping-based locomotion of animals

The flapping-based locomotion is often utilized by swimming and flying animals.[1–3,80] Based on the above results, we further discuss how quantities such as the bending stiffness K, the passive pitching angle α_{rms}, and the Strouhal number St are related to animal locomotion.

We first discuss the connection of the bending rigidity K and the flapping-based locomotion. Based on experimental data for some swimming and flying animals,[62, 68, 70, 81] we can estimate the
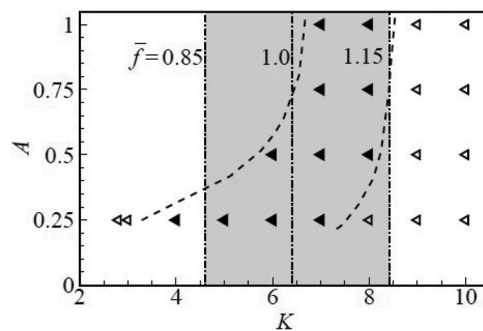
FIG. 15. Overview of the normal and deflected wakes in the FM region based on some typical cases simulated in this study. Symbols $\lhd$ and $\blacktriangleleft$ represent the normal and deflected wakes, respectively. Dashed lines represent approximately the boundaries between the two kinds of wakes. Dashed dotted lines denote different values of the frequency ratio $\bar{f}$.

bending stiffness of tail-fins or wings, e.g., $K \simeq 25$–230 for the tail-fin of a goldfish (*Carassius auratus*), 67 for the wing of a crane fly (*Tipula obsoleta*), and 49 for the wing of a dragonfly (*Aeschna juncea*). For comparison, as shown in Figs. 7 and 8, the large forward speeds and high propulsive efficiencies correspond to the range of $K \simeq 30$–200. This is in good agreement with the values obtained above for the real tail-fins and wings.

Then we address the pitching angle α_{rms}. From Figs. 7, 8, and 11, the range of $\alpha_{rms} = 5°$–25° is associated with the large forward speed and high propulsive efficiency. Fish[64] filmed the cruise swimming of bottlenose dolphins (*Tursiops truncatus*) and identified the angle between the tangent of the flukes' path and the axis of the flukes. He identified that the maximum angle of attack of the flukes ranged between 5° and 30°. To mimic the locomotion of tail-fins in swimming animals,[13,69] a harmonically oscillating foil in uniform flow was investigated experimentally and the pitching angle with optimum propulsive performance was found to be within 15°–25°. Our numerical results are consistent with these data.

Finally we analyze the relationship between the Strouhal number St and the animal locomotion. Usually, St is referred to as an appropriate parameter governing propulsive performance. Based on investigations of 42 species (birds, bats, insects, sharks, bony fish, and dolphins) in the cruise state, Taylor *et al.*[65] statistically estimated that St lies in the interval $0.2 < St < 0.4$. In this range, the cruise of the flying and swimming animals driven by the wing or tail is likely to have high propulsive efficiency. For a flapping foil in a uniform flow, the efficiency is higher than the range of $0.2 < St < 0.4$.[12,13,69] For comparison, our present numerical results in Fig. 12 indicate that the high propulsive efficiencies occur approximately when $St = 0.2$–0.4. In addition, St is also known to govern a well-defined series of regimes for vortex growth and shedding of a flapping wing. When $St = 0.2$–0.4, a reverse von Kármán vortex street is formed in the wake, which is related to the thrust production in the animal locomotion.

V. CONCLUDING REMARKS

The locomotion of a flapping flexible plate in a stationary viscous fluid has been studied by the immersed boundary-lattice Boltzmann method and the finite element method for numerical solutions of the coupled motions of the fluid and plate. Numerous simulations using a wide range of parameters are performed and various mechanisms governing the dynamics of the flapping flexible plate are investigated. Here we briefly summarize the results relevant to the flapping-based locomotion of swimming and flying animals.

We have found three distinct dynamic states of the plate motion, i.e., forward, backward, and irregular. Which state to occur mainly depends on the heaving amplitude and the bending rigidity of the plate. The diagram of the three states is obtained on the K–A plane. It is noticed that the region of the forward state covers a majority of the K–A plane while the region of the backward state covers a minority of the plane. When the heaving amplitude is large enough, only the forward and backward states appear; when the amplitude is small enough, only the forward state occurs.

The dynamical behaviors and propulsive properties of the flapping flexible plate in the forward motion regime have been investigated in detail. The study of the effect of the bending stiffness K on the propulsion of the plate indicates that a suitable degree of flexibility can improve the propulsive performance in terms of larger forward speed and higher propulsive efficiency. The elastic potential energy of the flexible plate is closely related to its propulsive properties. Moreover, it is obtained that larger heaving amplitude or smaller bending modulus causes more delay in the motion of the free end of the plate, therefore results in larger pitching angle which affects the dynamical behaviors of the flexible plate.

The vortical structure in the wake is investigated since it affects the motion and deformation of the plate. Both normal and deflected wakes are identified in the forward motion regime. Because of the deflection of the reverse von Kármán vortex street, the mean lift and thrust on the plate are generated. The Strouhal number St is a parameter governing a well-defined series of regimes for vortex growth and shedding of a flapping wing. When $St = 0.2$–0.4, corresponding to the range adopted by the swimming and flying animals, a reverse von Kármán vortex street occurs, which is associated with the thrust generation in animal locomotion. Moreover, the force and power of the

flapping plate mainly depend on the attached vorticity and the local vortical structure close to the plate.

Further, we have discussed the relationships between our computational results and animal's flapping-based locomotion in terms of the bending stiffness K, the passive pitching angle α_{rms}, and the Strouhal number St. The comparison and discussion indicate that our numerical results are consistent with those of the observations and measurements of swimming and flying animals. Therefore, our computational studies have provided some physical insights into the understanding of the propulsive mechanisms of the flapping wings and fins. Nevertheless, the flow involved in animal locomotion is far more complex and diverse than the flow involved in the flapping of a flexible plate considered here. Detailed investigation of viscous flows around flexible bodies in three dimensions is still needed in future work.

ACKNOWLEDGMENTS

[1] R. W. Blake, *Fish Locomotion* (Cambridge University Press, Cambridge, 1983).

[2] J. J. Videler, *Fish Swimming* (Chapman and Hall, New York, 1993).

[3] A. K. Brodsky, *The Evolution of Insect Flight* (Oxford University Press, Oxford, 1994).

[4] S. A. Combes and T. L. Daniel, "Flexural stiffness in insect wings. I. Scaling and the influence of wing venation," J. Exp. Biol. **206**, 2979–2987 (2003).

[5] S. A. Combes and T. L. Daniel, "Flexural stiffness in insect wings. II. Spatial distribution and dynamic wing bending," J. Exp. Biol. **206**, 2989–2997 (2003).

[6] R. J. Wootton, "Invertebrate paraxial locomotory appendages: Design, deformation and control," J. Exp. Biol. **202**, 3333–3345 (1999).

[7] F. E. Fish and G. V. Lauder, "Passive and active flow control by swimming fishes and mammals," Annu. Rev. Fluid Mech. **38**, 193–224 (2006).

[8] W. Shyy, Y. Lian, J. Tang, D. Viieru, and H. Liu, *Aerodynamics of Low Reynolds Number Flyers* (Cambridge University Press, Cambridge, 2008).

[9] W. Shyy, H. Aono, S. K. Chimakurthi, P. Trizila, C.-K. Kang, C. E. S. Cesnik, and H. Liu, "Recent progress in flapping wing aerodynamics and aeroelasticity," Prog. Aerosp. Sci. **46**, 284–327 (2010).

[10] R. J. Wootton, R. C. Herbert, P. G. Young, and K. E. Evans, "Approaches to structural modeling of insect wings," Philos. Trans. R. Soc. London, Ser. B **358**, 1577–1587 (2003).

[11] S. Alben, P. G. Madden, and G. V. Lauder, "The mechanics of active fin-shape control in ray-finned fishes," J. R. Soc., Interface **4**, 243–256 (2007).

[12] M. S. Triantafyllou, G. S. Triantafyllou, and R. Gopalkrishnan, "Wake mechanics for thrust generation in oscillating foils," Phys. Fluids **3**, 2835–2837 (1991).

[13] J. M. Anderson, K. Streitlien, D. S. Barrett, and M. S. Triantafyllou, "Oscillating foils of high propulsive efficiency," J. Fluid Mech. **360**, 41–72 (1998).

[14] N. Vandenberghe, J. Zhang, and S. Childress, "Symmetry breaking leads to forward flapping flight," J. Fluid Mech. **506**, 147–155 (2004).

[15] N. Vandenberghe, S. Childress, and J. Zhang, "On unidirectional flight of a free flapping wing," Phys. Fluids **18**, 014102 (2006).

[16] R. Godoy-Diana, J.-L. Aider, and J. E. Wesfreid, "Transitions in the wake of a flapping foil," Phys. Rev. E **77**, 016308 (2008).

[17] J. H. Buchholz and A. J. Smits, "The wake structure and thrust performance of a rigid low-aspect-ratio pitching panel," J. Fluid Mech. **603**, 331–365 (2008).

[18] M. J. Lighthill, "Note on the swimming of slender fish," J. Fluid Mech. **9**, 305–317 (1960).

[19] T. Y.-T. Wu, "Swimming of a waving plate," J. Fluid Mech. **10**, 321–344 (1961).

[20] J.-Y. Cheng, L.-X. Zhuang, and B.-G. Tong, "Analysis of swimming three-dimensional waving plates," J. Fluid Mech. **232**, 341–355 (1991).

[21] Z. J. Wang, "Vortex shedding and frequency selection in flapping fight," J. Fluid Mech. **410**, 323–341 (2000).

[22] Z. J. Wang, "Two dimensional mechanism for insect hovering," Phys. Rev. Lett. **85**, 2216 (2000).

[23] H. Dong, R. Mittal, and F. M. Najjar, "Wake topology and hydrodynamic performance of low-aspect-ratio flapping foils," J. Fluid Mech. **566**, 309–343 (2006).

[24] J. Carling, T. L. Williams, and G. Bowtell, "Self-propelled anguilliform swimming: Simultaneous solution of the two-dimensional Navier-Stokes equations and Newton's laws of motion," J. Exp. Biol. **201** (1998).

[25] S. Alben and M. Shelley, "Coherent locomotion as an attracting state for a free flapping body," Proc. Natl Acad. Sci. U.S.A. **102**, 11163 (2005).

[26] S. Kern and P. Koumoutsakos, "Simulations of optimized anguilliform swimming," J. Exp. Biol. **209**, 4841–4857 (2006).

[27] X.-Y. Lu and Q. Liao, "Dynamic responses of a two-dimensional flapping foil motion," Phys. Fluids **18**, 098104 (2006).

28 X. Zhang, S. Z. Ni, S. Z. Wang, and G. W. He, "Effects of geometric shape on the hydrodynamics of a self-propelled flapping foil," Phys. Fluids **21**, 103302 (2009).

29 I. Borazjani and F. Sotiropoulos, "On the role of form and kinematics on the hydrodynamics of self-propelled body/caudal fin swimming," J. Exp. Biol. **213**, 89–107 (2010).

30 Q. Zhu, "Optimal frequency for flow energy harvesting of a flapping foil," J. Fluid Mech. **675**, 495–517 (2011).

31 S. Heathcote and I. Gursul, "Flexible flapping airfoil propulsion at low Reynolds numbers," AIAA J. **45**, 1066–1079 (2007).

32 S. Heathcote, Z. Wang, and I. Gursul, "Effect of spanwise flexibility on flapping wing propulsion," J. Fluids Struct. **24**, 183–199 (2008).

33 S. Michelin and S. G. L. Smith, "Resonance and propulsion performance of a heaving flexible wing," Phys. Fluids **21**, 071902 (2009).

34 J. D. Eldredge, J. Toomey, and A. Medina, "On the roles of chord-wise flexibility in a flapping wing with hovering kinematics," J. Fluid Mech. **659**, 94–115 (2010).

35 P. J. S. A. Ferreira de Sousa and J. J. Allen, "Thrust efficiency of harmonically oscillating flexible flat plates," J. Fluid Mech. **674**, 43–66 (2011).

36 C.-K. Kang, H. Aono, C. E. S. Cesnik, and W. Shyy, "Effects of flexibility on the aerodynamic performance of flapping wings," J. Fluid Mech. **689**, 32–74 (2011).

37 T. Y.-T. Wu, "On theoretical modeling of aquatic and aerial animal locomotion," Adv. Appl. Mech. **38**, 291–353 (2002).

38 E. D. Tytell, C. Y. Hsu, T. L. Williams, A. H. Cohen, and L. J. Fauci, "Interactions between internal forces, body stiffness, and fluid environment in a neuromechanical model of lamprey swimming," Proc. Natl Acad. Sci. U.S.A. **107**, 19832 (2010).

39 S. E. Spagnolie, L. Moret, M. J. Shelley, and J. Zhang, "Surprising behaviors in flapping locomotion with passive pitching," Phys. Fluids **22**, 041903 (2010).

40 J. Zhang, N.-S. Liu, and X.-Y. Lu, "Locomotion of a passively flapping flat plate," J. Fluid Mech. **659**, 43–68 (2010).

41 L. Zhu and C. S. Peskin, "Simulation of a flapping flexible filament in a flowing soap film by the immersed boundary method," J. Comput. Phys. **179**, 452–468 (2002).

42 B. S. H. Connell and D. K. P. Yue, "Flapping dynamics of a flag in a uniform stream," J. Fluid Mech. **581**, 33–67 (2007).

43 C. S. Peskin, "The immersed boundary method," Acta Numer. **11**, 479–517 (2002).

44 R. Mittal and G. Iaccarino, "Immersed boundary methods," Annu. Rev. Fluid Mech. **37**, 239–261 (2005).

45 D. Goldstein, R. Handler, and L. Sirovich, "Modeling a no slip flow boundary with an external force field," J. Comput. Phys. **105**, 354–366 (1993).

46 W.-X. Huang, S. J. Shin, and H. J. Sung, "Simulation of flexible filaments in a uniform flow by the immersed boundary method," J. Comput. Phys. **226**, 2206–2228 (2007).

47 W.-X. Huang and H. J. Sung, "Three-dimensional simulation of a flapping flag in a uniform flow," J. Fluid Mech. **653**, 301–336 (2010).

48 T. Gao and X.-Y. Lu, "Insect normal hovering flight in ground effect," Phys. Fluids **20**, 087101 (2008).

49 F.-B. Tian, H. Luo, L. Zhu, and X.-Y. Lu, "Coupling modes of three filaments in side-by-side arrangement," Phys. Fluids **23**, 111903 (2011).

50 S. Chen and G. D. Doolen, "Lattice Boltzmann method for fluid flows," Annu. Rev. Fluid Mech. **30**, 329–364 (1998).

51 C. K. Aidun, Y. Lu, and E.-J. Ding, "Direct analysis of particulate suspensions with inertia using the discrete Boltzmann equation," J. Fluid Mech. **373**, 287–311 (1998).

52 Z. Xia, K. W. Connington, S. Rapaka, P. Yue, J. J. Feng, and S. Chen, "Flow patterns in the sedimentation of an elliptical particle," J. Fluid Mech. **625**, 249–272 (2009).

53 Z. Guo, C. Zheng, and B. Shi, "Discrete lattice effects on the forcing term in the lattice boltzmann method," Phys. Rev. E **65**, 046308 (2002).

54 Y. Cheng and J. Li, "Introducing unsteady non-uniform source terms into the lattice Boltzmann model," Int. J. Numer. Methods Fluids **56**, 629–641 (2008).

55 D. Yu, R. Mei, and W. Shyy, "A multi-block lattice Boltzmann method for viscous fluid flows," Int. J. Numer. Methods Fluids **39**, 99–120 (2002).

56 Y. Peng, C. Shu, Y. T. Chew, X. D. Niu, and X.-Y. Lu, "Application of multi-block approach in the immersed boundary¨-clattice Boltzmann method for viscous fluid flows," J. Comput. Phys. **218**, 460–478 (2006).

57 C. Pacoste, "Co-rotational flat facet triangular elements for shell instability analyses," Comput. Methods Appl. Mech. Eng. **156**, 75–110 (1998).

58 J. F. Doyle, *Nonlinear Analysis of Thin-Walled Structures: Statics, Dynamics, and Stability* (Springer-Verlag, New York, 2001).

59 B. Yin and H. Luo, "Effect of wing inertia on hovering performance of flexible flapping wings," Phys. Fluids **22**, 111902 (2010).

60 F.-B. Tian, H. Luo, L. Zhu, J. C. Liao, and X.-Y. Lu, "An efficient immersed boundary-lattice Boltzmann method for the hydrodynamic interaction of elastic filaments," J. Comput. Phys. **230**, 7266–7283 (2011).

61 B. Richard, "The speed of swimming of fish as related to size and to the frequency and amplitude of the tail beat," J. Exp. Biol. **35**, 109–133 (1958).

62 C. P. Ellington, "The aerodynamics of hovering insect flight. II. Morphological parameters," Philos. Trans. R. Soc. London, Ser. B **305**, 17–40 (1984).

63 C. P. Ellington, "The aerodynamics of hovering insect flight. III. Kinematics," Philos. Trans. R. Soc. London, Ser. B **305**, 41–78 (1984).

64 F. E. Fish, "Power output and propulsive efficiency of swimming bottlenose dolphins (*Tursiops truncatus*)," J. Exp. Biol. **185**, 179–193 (1993).

[65] G. K. Taylor, R. L. Nudds, and A. L. R. Thomas, "Flying and swimming animals cruise at a Strouhal number tuned for high power efficiency," Nature (London) **425**, 707–711 (2003).

[66] S. A. Combes and T. L. Daniel, "Into thin air: Contributions of aerodynamic and inertial-elastic forces to wing bending in the hawkmoth *Manduca sexta*," J. Exp. Biol. **206**, 2999–3006 (2003).

[67] J.-S. Chen, J.-Y. Chen, and Y.-F. Chou, "On the natural frequencies and mode shapes of dragonfly wings," J. Sound Vib. **313**, 643–654 (2008).

[68] S. R. Jongerius and D. Lentink, "Structural analysis of a dragonfly wing," Exp. Mech. **50**, 1323–1334 (2010).

[69] M. S. Triantafyllou, G. S. Triantafyllou, and D. K. P. Yue, "Hydrodynamics of fishlike swimming," Annu. Rev. Fluid Mech. **32**, 33–53 (2000).

[70] D. Ishihara, T. Horie, and M. Denda, "A two-dimensional computational study on the fluid-structure interaction cause of wing pitch changes in dipteran flapping flight," J. Exp. Biol. **212**, 1–10 (2009).

[71] W. T. Thomson, *Theory of Vibration with Applications* (Prentice-Hall, Englewood Cliffs, NJ, 1981).

[72] W. W. Schultz and P. W. Webb, "Power requirements of swimming: Do new methods resolve old questions?" Integr. Comp. Biol. **42**, 1018–1025 (2002).

[73] L. Zhu, "Interaction of two tandem deformable bodies in a viscous incompressible flow," J. Fluid Mech. **635**, 455–475 (2009).

[74] S. Bagheri, A. Mazzino, and A. Bottaro, "Spontaneous symmetry breaking of a hinged flapping filament generates lift," Phys. Rev. Lett. **109**, 154502 (2012).

[75] W. C. Young and R. Budynas, *Roark's Formulas for Stress and Strain* (McGraw-Hill, New York, 2001).

[76] J.-Z. Wu, X.-Y. Lu, and L.-X. Zhuang, "Integral force acting on a body due to local flow structures," J. Fluid Mech. **576**, 265– 286 (2007).

[77] G.-J. Li and X.-Y. Lu, "Force and power of flapping plates in a fluid," J. Fluid Mech. **712**, 598–613 (2012).

[78] K. D. Jones, C. M. Dohring, and M. F. Platzer, "Experimental and computational investigation of the Knoller-Betz effect," AIAA J. **36**, 1240–1246 (1998).

[79] G. C. Lewin and H. Haj-Hariri, "Modelling thrust generation of a two-dimensional heaving airfoil in a viscous flow," J. Fluid Mech. **492**, 339–362 (2003).

[80] S. Vogel, *Life in Moving Fluids* (Princeton University Press, Princeton, 1994).

[81] S. A. Wainwright, W. D. Biggs, J. D. Currey, and J. M. Gosline, *Mechanical Design in Organisms* (Princeton University Press, Princeton, 1982).